13th World Conference on Earthquake Engineering
Vancouver, B.C., Canada
August 1-6, 2004
Paper No. 2359

DYNAMIC FAILURE AND DEFORMATIONS OF DAM-MODELS ON SHAKING TABLE TESTS

Susumu MASUKAWA[1], Masami YASUNAKA[2] and Yuji KOHGO[3]

SUMMARY

Strong motions including vertical ones such as 1995 Hyogo-ken Nambu Earthquake were subjected to embankments of dams. Shaking table tests for the dam models were conducted to investigate failure and deformation behavior of the embankments due to strong ground motions including vertical ones.

In the tests, two cases (H and HV) were adopted. Horizontal direction waves were applied in the H cases, while horizontal and vertical direction waves were applied in the HV cases. The dimensions of the models were 80cm in height, 360cm in length at the crest. The models were constructed by compacting Japanese standard sand called Toyoura sand with 5% water contents. The amplitude of Acceleration applied was gradually increased 100Gal until the collapse of the dam models.

Deformations and acceleration were measured during the tests. The deformations were measured with laser displacement devices, video cameras and special designed ground strain instruments installed within the embankments and on the surface of models. Slip lines and failure situations were identified on some sections after tests.

The magnitudes of acceleration at the failure in the H and HV cases were 600 and 500Gal, respectively. In both cases, longitudinal cracks occurred on the slopes and the crests. Slides finally occurred. These longitudinal cracks appeared by an even interval and crossed perpendicular to the slopes. The cracks progressed toward the center of the models. The cracks might be induced by tension. The vertical motion induced greater tensile force on the slopes in HV cases than those in H cases. Deformations measured by the special designed ground strain instruments leaned somewhat toward the upper of slope immediately after shaking start. Following those, deformations became bending toward the lower of slope by sliding. Deformations measured by the special designed ground strain instruments were consistent with bending shape of these instruments after shaking.

The longitudinal cracks on the slopes and the crests did not always induce the slide. These cracks were caused by tensile forces on the slopes. These tensile forces acting on the slopes of the models with both horizontal and vertical motions became larger than those with only horizontal motion. The special designed ground strain instruments could measure sliding deformations precisely.

---

[1]Research Engineer, National Institute for Rural Engineering, Tsukuba, Japan.
Email: susumu@nkk.affrc.go.jp

[2]Chief of Research and Development Division, Agriculture, Forestry and Fisheries Research Council Secretariat, Ministry of A.F.F., Tokyo, Japan

[3]Head of Structural Analysis Lab., National Institute for Rural Engineering, Tsukuba, Japan.

INTRODUCTION

During the 1995 Hyogoken-Nambu Earthquake, dams were subjected to strong motions generated from active faults in its hypocenter. It is necessary to evaluate the safety of dams subjected to such strong motions, including vertical ones by considering the dynamic deformations of dams. The phenomenon of dynamic progressive failure needs to be clarified in order to predict dynamic deformations taking into account the modes of failure. We conducted two series of shaking table test for models of an earthfill dam in order to identify the influence of vertical motion on the dam models. The tests consisted of two cases: H case, in which the model is shaken only to the upstream-downstream direction, and HV case, in which it is shaken simultaneously to the upstream-downstream and the vertical directions.

OUTLINE OF THE EARTHFILL DAM MODEL

Centrifuge tests, which are used to clarify the behavior of dynamic failure of a soil structure, are known to satisfy the law of similarity and are therefore superior to a 1g shaking table test. However, in granular materials such as sand, it is known that the particle size effect, which represents increasing particle size relative to centrifuge acceleration, influences to shear banding[1]. Therefore, we conducted a 1g shaking table test with model dams in order to reproduce more accurately the failure phenomenon with the shear banding.

The material, water content, and relative density for the model tests were set through preliminary tests using various small model dams. Model dam embankments compacting Japanese standard sand, Toyoura sand, with a 5% water content, were appropriate for observing the cracking condition and slip lines. The properties of Toyoura sand are shown in Table 1.

Table 1 Properties of Toyoura sand

Mineral composition	Uniformity coefficient	Coefficient of curvature	Density (g/cm^3)	Minimum dry density (g/cm^3)	Maximum dry density (g/cm^3)
Quartz	1.46	0.96	2.643	1.337	1.646

The dam models did not represent scale down models of a prototype dam. They were prepared to clarify the effects of vertical vibration on the collapse of the dam models. Therefore the dam models only consist of embankments without foundations and reservoirs. Two degrees of compaction were set, 0% and 50% so that the models had the different shear strength. The dimensions of the dam models are 80 cm in height, 364 cm in crest length, and 1:1.5 slopes. Two model shapes were prepared: a two dimensional model (2D model) and a pseudo-three dimensional model (3D model). The 3D model had a 45° slope of abutment on one side and contacted with the vertical glass surface on the other side. Both sides of the 2D model contacted with vertical surfaces and were fixed. This model therefore satisfied the plane strain condition. The model specifications are shown in Table 2, and their dimensions are shown in Fig. 1.

Table 2 Specifications of model dams

Case No.	Shape	Shaking direction	Water contents (%)*	Dry density (g/cm^3) *	Relative density (%)*
Case 9	2D model	H	5 (5.0)	1.48 (1.40)	50 (51)
Case 8	3D model		5 (4.7)	1.48 (1.42)	50 (51)
Case 1	3D model	HV	5 (4.6)	1.48 (1.43)	50 (35)
Case 3	3D model		5 (5.5)	1.34 (1.31)	0 (0)

* The values in parentheses are measured after tests

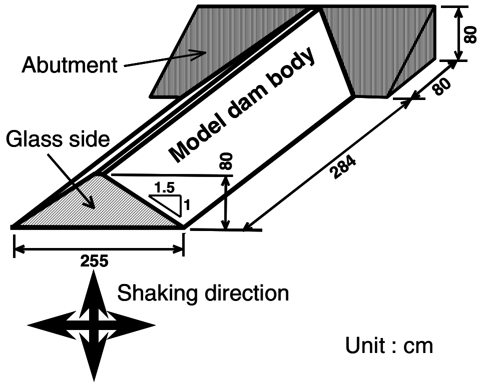

Fig. 1 Shape of model dam (3D model)

OUTLINE OF SHAKING TABLE TEST

Acceleration during shaking, displacements (on the surfaces and within the embankments), cracks and shapes of the slip surfaces on the excavated cross section after tests were measured. Input acceleration and response acceleration were measured by strain gauge type accelerometers. Displacements were evaluated by measuring the movements of markers installed on the model surfaces and within the embankments. Displacements during shaking were measured with laser assisted displacement gauges and strain measuring instruments installed into the embankments. The strain measuring instrument was made of a strip of a plastic board with 2 mm thickness and 60 cm length. Strain gauges were attached on both sides of the strip at intervals of 8 cm. One end of the strain measuring instrument was fixed to the bottom of the shaking table, and was perpendicularity installed within the embankments. The strain measuring instruments measured slidings as bending strains. Figure 2 shows the layout of the laser assisted displacement gauges and Fig. 3 shows the outline of the strain measuring instrument.

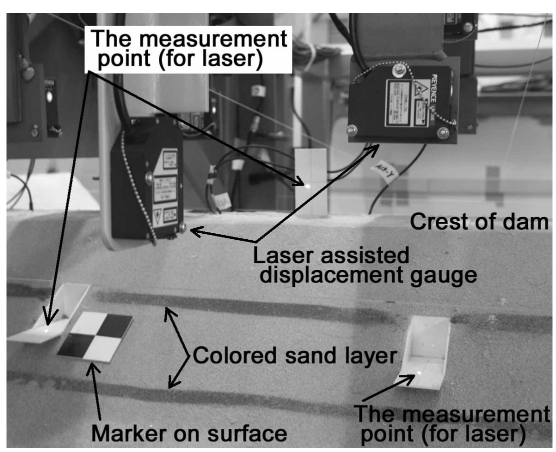

Fig. 2 Laser assisted displacement gauges

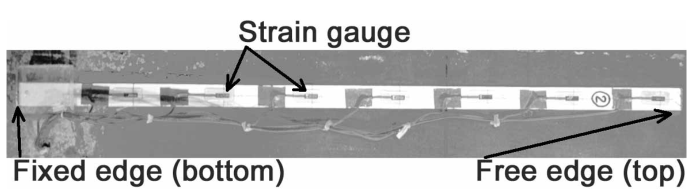

Fig. 3 Outline of the strain measuring instrument

Colored sand layers were inserted at every 10 cm layers to observe slip. A video camera was used to record how cracks and slidings occurred during the shakings. Every model had a little bit different arrangement of the measuring points. The typical arrangement of the measuring points is shown in Figs. 4 to 7. The input waves were 5, 10 or 15 Hz sine waves with the acceleration amplitude ± 300 to 600 Gal. Table 3 shows the shaking conditions. For stable shaking control, five tapered waves were used from 0 Gal to the predetermined acceleration amplitude. The amplitude was gradually increased 100 Gal each until the collapse of the dam model. Each wave was kept for 30 seconds at maximum. Shaking was stopped when a sliding was visually observed. In HV case, there was no phase difference between horizontal and vertical direction waves. Then, the acceleration vector occupied the direction of 45° relative to the horizontal surface (Fig. 8).

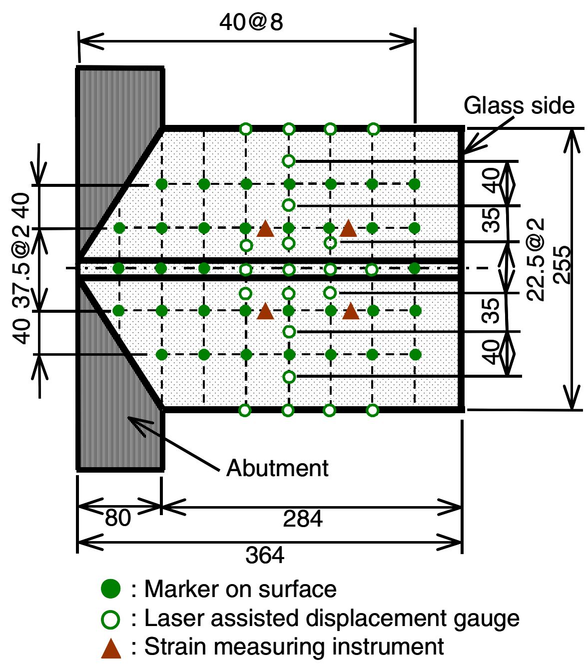

Fig. 4 Arrangement of measuring points at projected longitudinal section

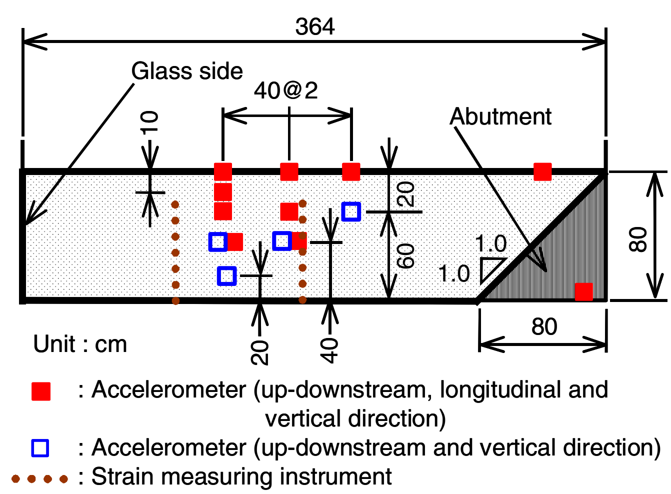

Fig. 5 Arrangement of measuring points at projected cross section

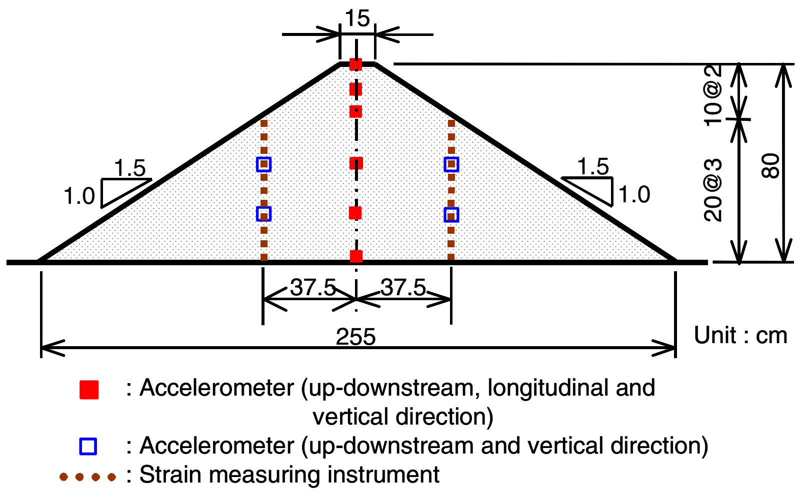

Fig. 6 Arrangement of measuring points at projected cross section

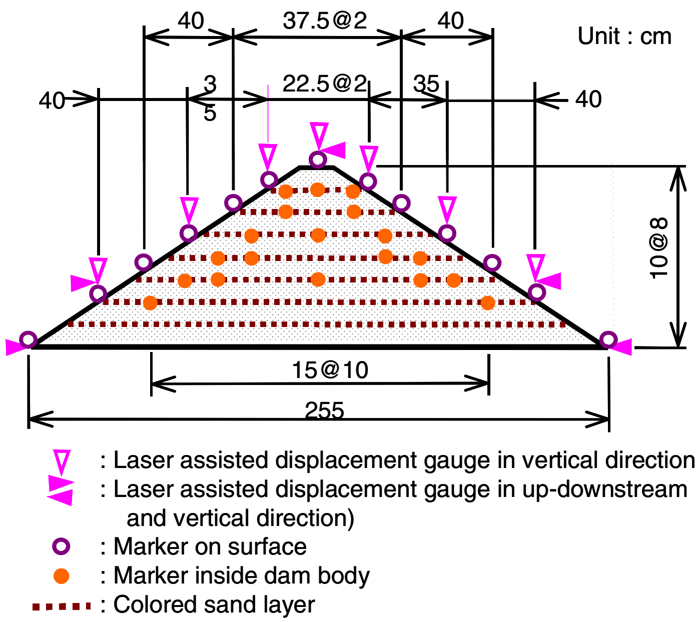

Fig. 7 Arrangement of measuring points at projected plane view

Table 3 Shaking conditions

Shaking direction	Shape	Case No.	Maximum acceleration and frequency			
H	2D model	Case 9	-	-	500Gal, 10Hz	600Gal, 10Hz (Collapse)
	3D model	Case 8	-	-	500Gal, 10Hz	600Gal, 10Hz (Collapse)
HV	3D model	Case 1	300Gal, 10Hz	400Gal, 10Hz	500Gal, 5Hz (Collapse)	-
	3D model	Case 3	-	400Gal, 10Hz	500Gal, 5Hz (Collapse)	-

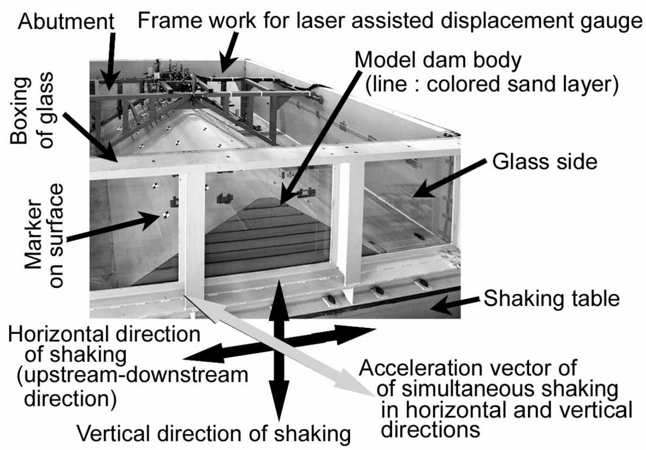

Fig. 8 Overview of shaking table test

COLLAPSE OF DAM MODELS

The dam models collapsed at the amplitude of 600Gal acceleration in H case and at 500 Gal in HV case (Table 3).

Figure 9 shows a plane view of the collapse in Case 1 (3D model). A large number of complex honeycomb-pattern cracks were seen on the crest. Cracks along the longitudinal direction also occurred on both slopes.

Figure 10 shows an excavated cross section in Case 3 (3D model). Slip lines toward both slopes were visually observed from sequential level differences of colored sand layers.

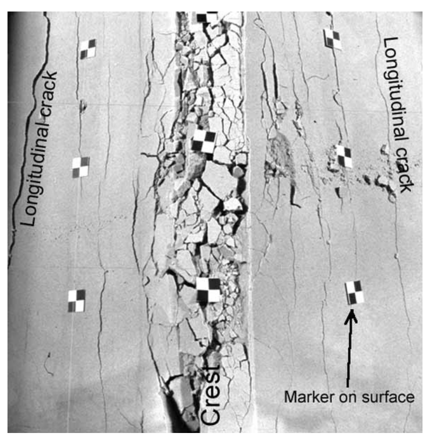

Fig. 9 Collapse in Case 1 (HV case, 3D model)

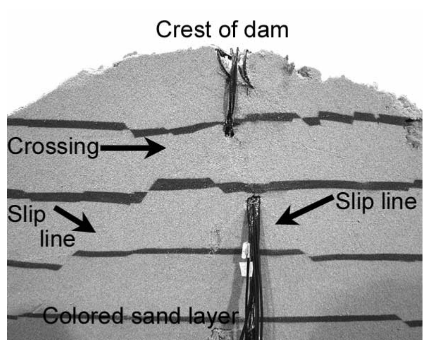

Fig. 10 Collapse at an excavated cross section in Case 3 (HV case, 3D model)

The collapse situations of all cases on excavated cross sections are shown in Figs. 11 to 14. The processes of collapse were apparently different between H cases and HV cases. For H cases, it was found from Figs. 11 and 12 that cracks first appeared on the crests toward the longitudinal direction. As these cracks developed, transverse cracks occurred, the occurrence of a few cracks toward the longitudinal direction on the slopes followed. Slidings on the left side slope occurred as shown in Figs. 11 and 12. Just after these slides on the left slopes, slides began on the right side slope. For HV cases, it was found from Fig. 13 and 14 that cracks first occurred toward the longitudinal direction on the slopes, the occurrence of cracks on the crest toward the longitudinal direction followed. As these cracks developed, transverse cracks occurred, slidings on the left side slope occurred as shown in Figs. 13 and 14. For Case 3, it was found from Fig. 14 that sliding also occurred on the right side slope. Just after this slid on the left slope, slides began on the right side slope. For H cases and HV cases, sliding does not move instantly, but sliding movement occurred while the sliding is being vibrated in synchronization with shaking waves. The slidings stopped as the shaking stopped.

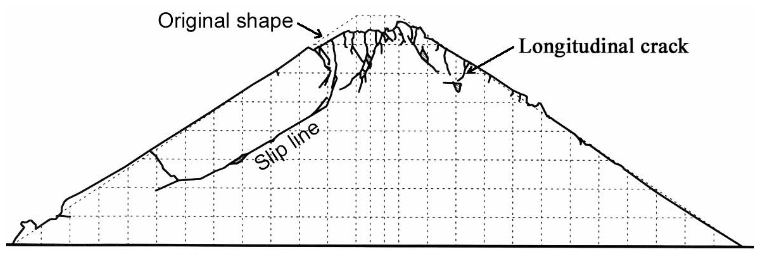

Fig. 11 Traced drawings at an excavated cross section in Case 9 (H case, 2D model)

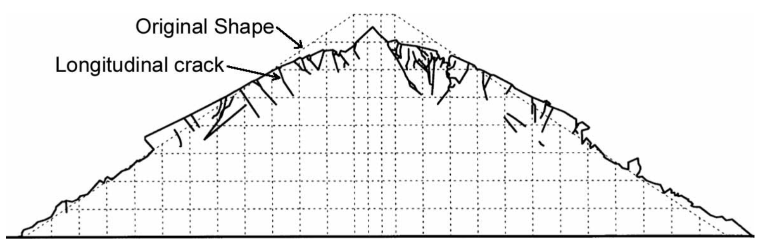

Fig. 12 Traced drawings at an excavated cross section in Case 8 (H case, 3D model)

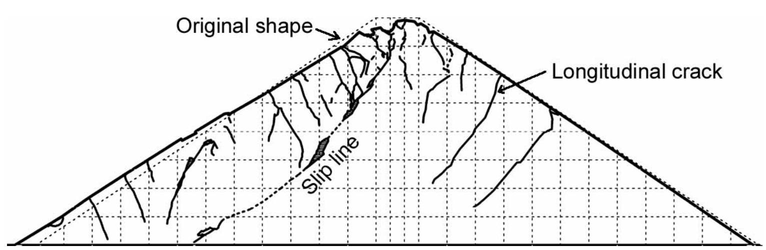

Fig. 13 Traced drawings at an excavated cross section in Case 1 (HV case, 3D model)

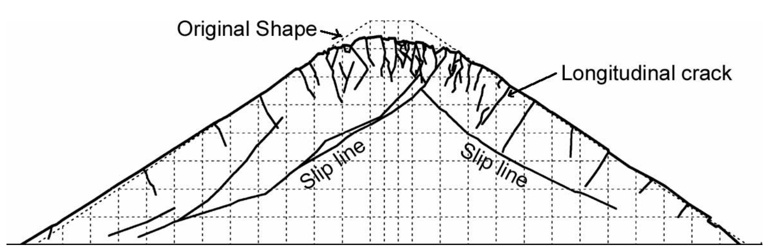

Fig. 14 Traced drawings at an excavated cross section in Case 3 (HV case, 3D model)

The collapse was characterized by cracks toward the longitudinal direction on slopes, as shown in Figs. 11 to 14. These cracks appeared before the slidings. More cracks toward the longitudinal direction were observed in HV cases than in H cases. In HV cases, after cracks toward longitudinal direction occurred on the slopes, the opening widths of the cracks increased during the shakings and new cracks toward the longitudinal direction appeared between the longitudinal cracks already existed. Eventually, longitudinal cracks occurred almost at an equal interval on the slopes. As shown in Figs. 11 to 14, the longitudinal cracks on the excavated cross sections in HV cases are longer and deeper than those in H cases, and they extended straightly. The vertical motion induced greater tensile forces on the slopes in HV cases than those in H cases.

A typical shape of longitudinal cracks, as described above, on the excavated cross section is shown in Fig. 15. The cracks traced on a line connecting two arrows shown in this figure. Triangles shown in this figure indicated that transverse cracks crossed the colored sand layers and there were no level differences of colored sand layers. Thus, it was concluded that the cracks toward the longitudinal direction were tensile cracks, not cracks caused by slidings.

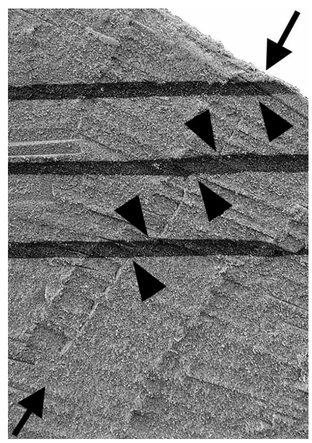

Fig. 15 Longitudinal crack at an excavated cross section in Case 1 (HV case, 3D model)

The characteristics of the slip lines in H cases and HV cases were the sliding that occurs just under the crests in a crisscross pattern (Figs. 11, 12 and 14). For Case 1 shown in Fig. 13, crack crossing the slip line were observed just under the crest as shown by Fig. 16.

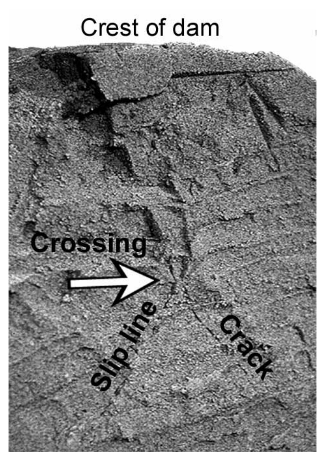

Fig. 16 Crossing crack just under the crest in Case 1 (HV case, 3D model)

DYNAMIC DEFORMATIONS

An example of measurement of dynamic displacements on the crest with a laser assisted displacement gauge is shown in Fig. 17. In this figure, the upper graph shows the relationship between settlement and shaking time and the lower one shows that between horizontal displacement and shaking time. Vibrational displacements associated with the input waves and residual deformations occurred during vibration. As shown in the figure, the settlement and the horizontal displacement did not suddenly occur. Furthermore, displacement increments per time decreased during shaking.

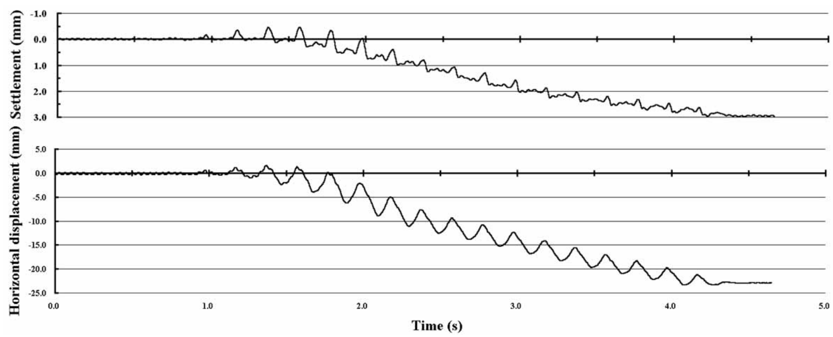

Fig. 17 Dynamic displacements measured by laser assisted displacement gauges on the crest

Dynamic displacements (Fig. 17) are shown as loci on the cross section in Figs. 18 to 20. Figures 18, 19 and 20 show the dynamic displacements on the crests of Cases 1, 3 and 9, respectively. For all three cases, since the slidings occurred on the left side slopes, as shown in Figs. 11, 13 and 14, the models also moved toward the left sides. The amounts of vibrational displacements among horizontal displacements were larger than those among the vertical ones. The similar phenomenon was also observed at measurement points on the crests in other cases. In Cases 1 and 9 shown in Figs. 18 and 20, the horizontal displacements were larger than the vertical ones (settlements) just after the start of the shakings and then settlements became larger. In Case 3 shown in Fig. 19, settlements began just after the start of the shakings and then horizontal displacement occurred. In addition, the amounts of vibrational displacements among the horizontal displacements were larger than those observed in other cases. The difference between Case 3 and Case 1 and 9 raises from the differences of relative densities of model.

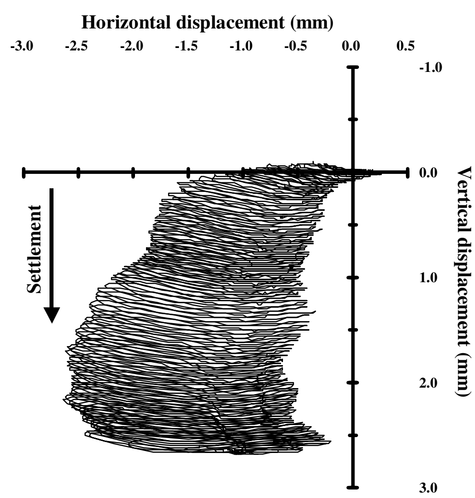

Fig. 18 Locus of dynamic displacements on the crest (Case 1)

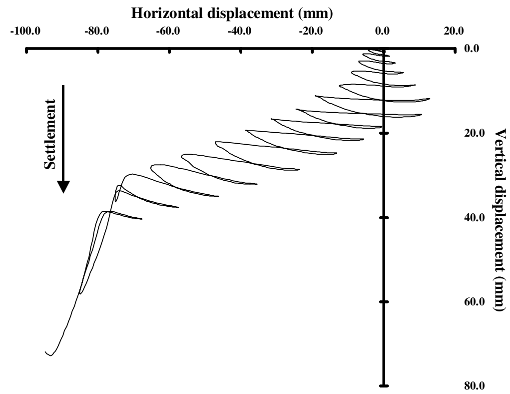

Fig. 19 Locus of dynamic displacements on the crest (Case 3)

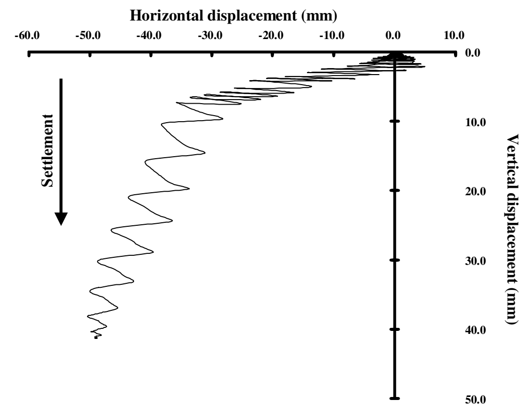

Fig. 20 Locus of dynamic displacements on the crest (Case 9)

Figure 21 shows the shape of the strain measuring instrument at an excavated cross section of Case 3. The strain measuring instrument was considerably bent at the points where the slip line crossed. Even in cases where no apparent slip line was observed, the strain measuring instruments were bent. Therefore, the positions of the slip lines could be clarified with the strain measuring instruments inside the embankments.

An example of measurement of bending strains using the strain measuring instrument inside the embankments is shown in Fig. 22. The figures sequentially ordered from top show the strain values at measuring points allocated from the top to the bottom of platen of the instruments. Vibrational components were also seen in the bending strains. Bending strains at the measuring points with 10 and 18 cm in depth increased at a constant rate, and then reached a large bending strain. This means that the platen of the instrument was bent near these measuring points.

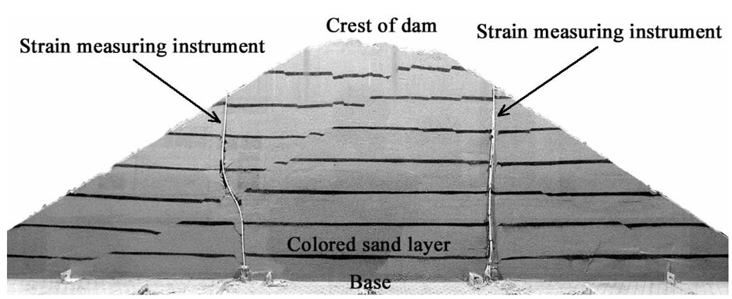

Fig. 21 Strain measuring instruments at an excavated cross section in Case 3

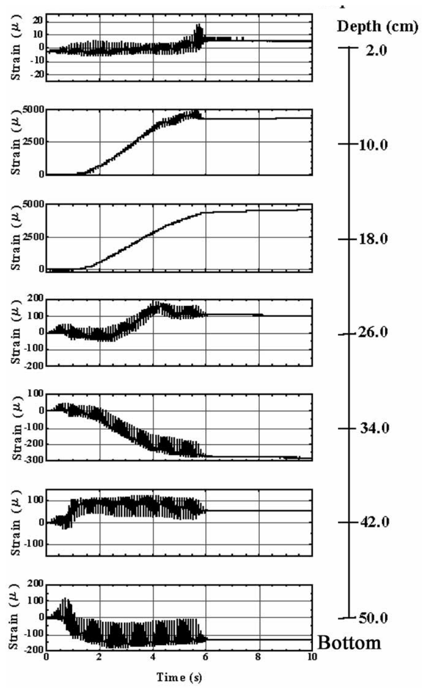

Fig. 22 Bending strains measured with strain measuring instrument

The bending strains measured with the strain measuring instruments were calculated horizontal displacements. The bending moments were also calculated from the bending strains. Spline functions were used to approximate the bending moments. The bending moments were integrated twice to obtain horizontal displacements. The displacements at the fixed edges of the strain measuring instruments were assumed to be 0. Figure 23 shows relationships between depth and the horizontal displacements calculated using data with the strain measuring instrument installed in the left side of the embankment for Case 8. This figure shows that the slid occurred within a period of 4 to 6 seconds after the shaking started.

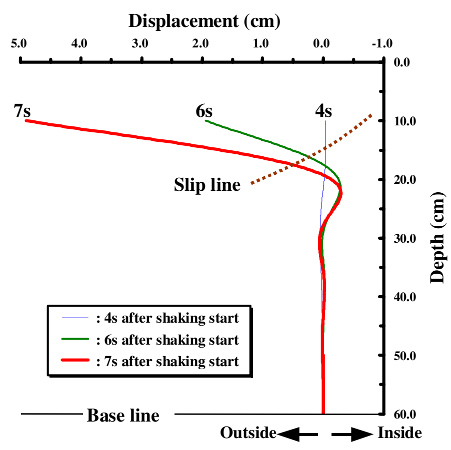

Fig. 23 Horizontal displacements inside the embankment (Case 8)

The bending strains measured by the strain measuring instrument inside the embankment in Fig. 21 also contains vibrational components, as displacements measured with the laser assisted displacement gauges shown in Fig. 17. Figure 24 shows horizontal displacements when the amplitude of bending strains at the lapse of 6, 8 and 10 seconds after shaking start was maximum or minimum. The measuring place in this figure was at the left side slope of Case 1. The amplitude at 8 seconds after the start of shaking became greater at than that at 6 seconds. Before shaking stopped (10 seconds), the amplitude was almost the same as that at the 8 seconds. This trend is the same as that in horizontal displacements, as measured by the laser assisted displacement gauges on the crests, in Figs. 19 and 20. Therefore, the slidings occurred with vibrating and the driving forces were inertial forces induced by the vibrations.

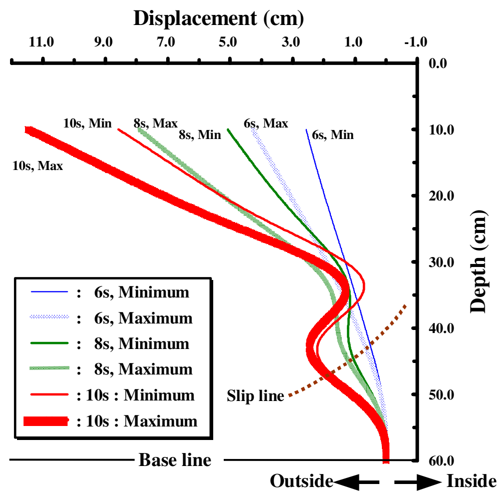

Fig. 24 Vibration components of horizontal displacements inside the embankment (Case 1)

Figure 25 shows changes in horizontal displacements by the strain measuring instrument installed in embankment at the right side slope of the excavated section for Case 8. The scale of horizontal displacements is enlarged and does not agree with the scale of the excavated section. The slip lines are shown as a dotted line in the figure. The bend existed at a depth of 10 cm from the slope surface within 5 to 6 seconds after shaking started. The bend then moved at a depth of about 20 cm from the slope surface within 8 to 10 seconds. The part of bent at depth of about 20cm agreed with the estimated slip line. Therefore, it is estimated that the slips occurred in two stages, namely, the sliding first occurred near the surface after the start of shaking and then occurred at a greater depth. Hence, the strain measuring instruments inside the embankments could accurately measure the condition of slip occurrence.

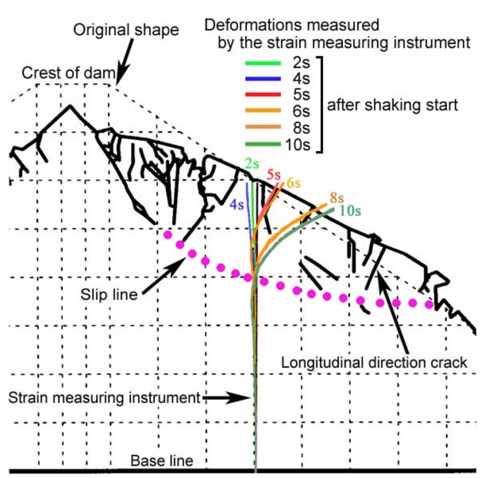

Fig. 25 Slip line and horizontal displacements inside the embankment (Case 8)

CONCLUSION

A series of shaking table tests were conducted for dam models simulating a homogeneous earthfill dam in order to clarify the influence of strong vertical motions and the phenomenon of dynamic progressive failure. The results of the tests indicated that the models with both horizontal and vertical motions failed under smaller acceleration amplitudes than those with only horizontal motion. It was also clarified that cracks occurred toward the longitudinal direction on the slopes before slidings. The longitudinal cracks were caused by tensile forces on the slopes. The results of tests indicated that the tensile forces acting on the slopes of the models with both horizontal and vertical motions became larger than those with only horizontal motion. Dynamic deformations occurred with response vibrations due to input waves. Resultant slidings were caused by inertial forces induced by shaking. The strain measuring instrument specially built for installation inside the embankment was capable of accurately monitoring the condition of slip occurrence and the position of the slip line during shaking.

REFERENCES

1. Siddiquee MSA, Tatsuoka F, Tanaka T, Tani K, Yoshida K, Morimoto T. “Model tests and FEM simulation of some factors affecting the bearing capacity of a footing on sand.” Soils and Foundations; 41(2), 53-76, 2001